INORGANIC CHEMISTRY
FRONTIERS

CHINESE CHEMICAL SOCIETY
ROYAL SOCIETY OF CHEMISTRY

RESEARCH ARTICLE

View Article Online
View Journal | View Issue

Published on 10 March 2023. Downloaded on 7/15/2025 3:38:55 AM.

Check for updates

Cite this: *Inorg. Chem. Front.*, 2023, **10**, 2414

Electroreduction of CO_2 to syngas with controllable H_2/CO ratios in a wide potential range over Ni–N co-doped ultrathin carbon nanosheets†

Kaining Gan, Hongqiang Li, * Ran Li, Jiabao Niu, Jun He, Dedong Jia and Xiaojun He *

Received 15th January 2023,
Accepted 9th March 2023

DOI: 10.1039/d3qi00108c

rsc.li/frontiers-inorganic

The conversion of CO_2 to syngas (H_2 and CO) *via* electrochemical reduction has been considered a promising strategy to mitigate the greenhouse effect. However, it is a great challenge to control H_2/CO ratios over a wide voltage window. Herein, a new method of fabricating Ni–N co-doped carbon nanosheets by molten salt-assisted pyrolysis, impregnation and re-carbonization is proposed. Benefiting from their ultrathin structure and tunable Ni–N_x active site content, the H_2/CO ratios can be adjusted from 1/2 to 2/1 within a wide applied voltage range (−0.7 to −1.3 V *vs.* RHE). After electrochemical stability testing for 10 h, the current density and H_2/CO ratios remained almost constant, revealing robust long-term stability. This work may benefit the construction of efficient and low-budget electrocatalysts for the production of tunable syngas.

Introduction

With the acceleration of industrialization, the excessive consumption of fossil fuels has caused an energy and environmental crisis.[1,2] To alleviate this problem, many emerging technologies such as capture and sequestration, chemical fixation, and electro/photochemical reduction have been proposed.[3,4] Of the above technologies, the electrochemical CO_2 reduction reaction (CO_2RR) has been regarded as a promising strategy for producing fuels and chemicals from renewable energy sources.[5] In recent years, considerable advances have been made in the CO_2RR, in which the reduction of CO_2 to low-carbon hydrocarbons is an intermediate step in the further production of high-value-added products.[6,7] Among them, syngas (H_2 and CO) is key feedstock for many important chemicals; for example, when the ratio of H_2/CO is 2/1, it is an ideal choice for methanol production while the optimal ratio for dimethyl ether production is 1/1.[8,9] Therefore, the realization of adjustable syngas production is very promising and also urgently needed.

In recent years, many attempts have been made to produce syngas *via* the CO_2RR. For instance, Kim *et al.* used Ag/TiO_2 as catalysts to produce tunable syngas.[10] These catalysts could regulate H_2/CO ratios from 0.1 to 1.5 by controlling oxygen vacancy contents in the range of applied potentials from −0.35 to −0.65 V (*vs.* RHE). He *et al.* developed Pd–SnO_2 nanosheet catalysts for syngas production with controllable H_2/CO ratios.[11] The large specific surface area of these catalysts exposes abundant active interfaces that can modulate the H_2/CO ratios from 0.28 to 4.2, when the potential is varied from −0.5 to −1.1 V (*vs.* RHE). However, precious metal catalysts have the disadvantages of high cost and scarce raw materials, which limit their large-scale application. Therefore, transition metal catalysts for electrosynthesis of syngas were also studied. Maeng *et al.* fabricated ZnO nanorod-based catalysts to prepare syngas.[12] By the surface modification of the employed catalysts, the H_2/CO ratios can be adjusted in the range of 0.25–4.5 within the applied potential range of −1.2 to −2.0 V (*vs.* Ag/AgCl). Chen *et al.* synthesized oxide-derived Cu nanowires with two-phase CuO heterostructures for syngas production.[13] Misfit dislocation sites on the surface of Cu nanowires promote the selectivity of CO, so that the H_2/CO ratios can be regulated from 1 to 3 within a certain potential window (−0.28 to −0.649 V *vs.* RHE). To further improve the stability of catalysts and reduce the cost, some researchers have developed carbon-based catalysts. Han *et al.* prepared BPNC catalysts for producing syngas *via* the CO_2RR.[14] By changing the precursor ratio of tetraphenylphosphonium tetraphenylborate ($C_{48}H_{40}BP$) to melamine, the H_2/CO ratios can be adjusted

---

School of Chemistry and Chemical Engineering, Anhui Key Laboratory of Coal Clean Conversion and High Valued Utilization, Key Laboratory of Metallurgical Emission Reduction & Resources Recycling, Ministry of Education, Anhui University of Technology, Maanshan 243002, P. R. China. E-mail: hqli2020@ahut.edu.cn, xjhe@ahut.edu.cn

† Electronic supplementary information (ESI) available. See DOI: https://doi.org/10.1039/d3qi00108c

This journal is © the Partner Organisations 2023

Published on 10 March 2023. Downloaded on 7/15/2025 3:38:55 AM.

from 0.2 to 6.8 in a potential window from −0.5 to −1.0 V (*vs.* RHE). Li *et al.* designed a series of nitrogen-doped carbon foam tubular electrodes to prepare syngas with controllable H_2/CO ratios.[15] These electrodes exhibit adjustable H_2/CO ratios (1/3 to 2/1) over a potential range from −0.5 to −1.3 V (*vs.* RHE). Inspired by the above research, the syngas ratio can be adjusted by regulating the number of active sites for CO production. Compared with the heteroatom-doped carbon catalysts, Ni–N-doped carbon materials have the advantages of higher atomic utilization, higher intrinsic activity and controllable active sites.[16–22] Benefiting from those merits, it is possible to control the amount of CO by regulating the number of Ni–N active sites, thereby adjusting the proportion of syngas.

Recently, Leverett *et al.* synthesized undercoordinated $Ni–N_x$ catalysts with a holey graphene framework to adjust the H_2/CO ratio by altering the coordination of Ni and N.[23] He *et al.* prepared N-doped carbon-supported single-atom catalysts CoNi-NC and regulated the syngas composition by controlling the doping ratio of Co to Ni.[24] Although the above studies have realized the regulation of the syngas ratios to some extent, the process of large-scale application of such catalysts is limited by the narrow adjustment ratio range or high cost of raw materials.

Herein, we synthesized Ni–N co-doped ultrathin carbon nanosheets by a molten salt-assisted pyrolysis, impregnation and re-carbonization strategy. The ultrathin structure of Ni–N co-doped carbon nanosheets can shorten the mass transfer path and provide a sufficient three-phase reaction interface for the CO_2RR. The number of Ni–N active sites can be adjusted by varying the carbonization temperature, thus enabling the adjustment of the CO yield and the regulation of the resulting syngas ratios. Therefore, the ratio of H_2/CO can be effectively regulated from 1/2 to 2/1 within a wide potential range (−0.70 to −1.30 V *vs.* RHE), which shows great promise for practical electrosynthesis of tunable syngas.

Results and discussion

The synthetic procedure of Ni/N–C is illustrated in Fig. 1a. In a typical process, coal tar pitch (carbon source) was mixed with salts (NaCl and KCl) and ground uniformly, followed by pyrolysis under an Ar atmosphere. During pyrolysis, the strong sheer force of the molten salts converted the pitch precursors into ultrathin carbon nanosheets. Subsequently, the as-prepared carbon nanosheets were treated with concentrated nitric acid to introduce nitro groups to facilitate Ni^{2+} adsorption. Then, Ni^{2+} was introduced into the carbon nanosheets by impregnation. The carbon nanosheets, after adsorption of Ni^{2+}, were then carbonized together with N sources under an Ar atmosphere. The product obtained after acid leaching and drying was labelled Ni/N–C. The Ni–C sample without the N source and the N–C sample without the Ni source were prepared by a similar route to demonstrate the significance of the interaction between N and Ni species. The structural characteristics of the obtained Ni/N–C-900 were examined by scanning electron microscopy (SEM) (Fig. 1b–d) and transmission electron microscopy (TEM) (Fig. 1e–g). Ni/N–C-900 clearly shows an ultrathin lamellar structure, which reduces the ion transport resistance and increases the accessible area of the active sites. Meanwhile, there was no metal aggregation in Ni/N–C-900. The N–C and Ni–C samples exhibit similar sheet-like structures to that of Ni/N–C-900 (Fig. S1†); the influence of material morphology on the catalytic performance can be excluded. Energy dispersive spectroscopy (EDS) mapping displays that N, O and Ni atoms were dispersed uniformly in the carbon nanosheets (Fig. 1h).

The microstructures of the Ni/N–C catalysts were further investigated by X-ray diffraction (XRD) (Fig. 2a). The XRD patterns of the Ni/N–C catalysts exhibit only two broad peaks located at around 26° and 44°, attributed to the (002) and (101) facets of graphite,[25] further suggesting the absence of metallic Ni nanoparticles in these catalysts. The crystal structure and defects of the prepared catalysts were evaluated with the Raman spectra. All the Ni/N–C catalysts show two characteristic bands at around 1340 cm^{-1} (D band) and 1580 cm^{-1} (G band) (Fig. 2b).[26–28]

Specifically, the I_D/I_G values of Ni/N–C-700, 800, 900 and 1000 are 0.94, 0.95, 0.97 and 0.96, respectively. The close I_D/I_G values of these four samples indicate that they all have similar graphitized structures, but these values are significantly higher than those of Ni–C (0.91) and N–C (0.93) (Fig. S2†), proving that the introduction of Ni–N active sites leads to an increase of disorder in carbon and thus more defects are obtained.[29]

To further reveal the elemental composition and coordination environment of Ni/N–C catalysts, X-ray photoelectron spectroscopy (XPS) measurements were carried out. The XPS wide-survey spectra of the Ni/N–C catalysts indicate the presence of C, N, O and Ni elements (Fig. S3†), which is in accordance with the EDS mapping. The C 1s spectra can be fitted into C–C (~284.6 eV), C–N (~285.6 eV) and C═O (~287.8 eV) (Fig. S4†), demonstrating that the N species are successfully doped into the carbon nanosheets.[30–32] As shown in Fig. 2c, the N 1s spectra can be deconvoluted into four peaks centered at 398.3 eV (pyridinic-N), 399.5 eV (Ni–N), 400.5 eV (pyrrolic-N) and 401.3 eV (graphitic-N).[33,34] The contents of various N species are shown in Fig. S5;† the pyridinic-N was dominant in all samples. More importantly, pyridinic-N has strong adsorption capacity for acidic CO_2 molecules, thus enhancing the CO_2RR rate.[14]

The Ni contents of the various samples characterized by XPS are 0.09 at% (Ni/N–C-700), 0.10 at% (Ni/N–C-800), 0.16 at% (Ni/N–C-900), and 0.13 at% (Ni/N–C-1000) (Table S1†), respectively, indicating that 900 °C is a potentially ideal temperature for preparing the Ni/N–C catalysts with relatively high Ni content. Meanwhile, we calculated the relative contents of nitrogen species in various Ni/N–C catalysts. Fig. S5† shows that the relative contents of pyridinic-N are 35.7, 33.3, 27.6 and 25.9%, when the carbonization temperature is 700, 800, 900 and 1000 °C, respectively. Meanwhile, the corresponding relative contents of pyrrolic-N are 21.3, 20.0, 17.6 and 17.3%,

Published on 10 March 2023. Downloaded on 7/15/2025 3:38:55 AM.

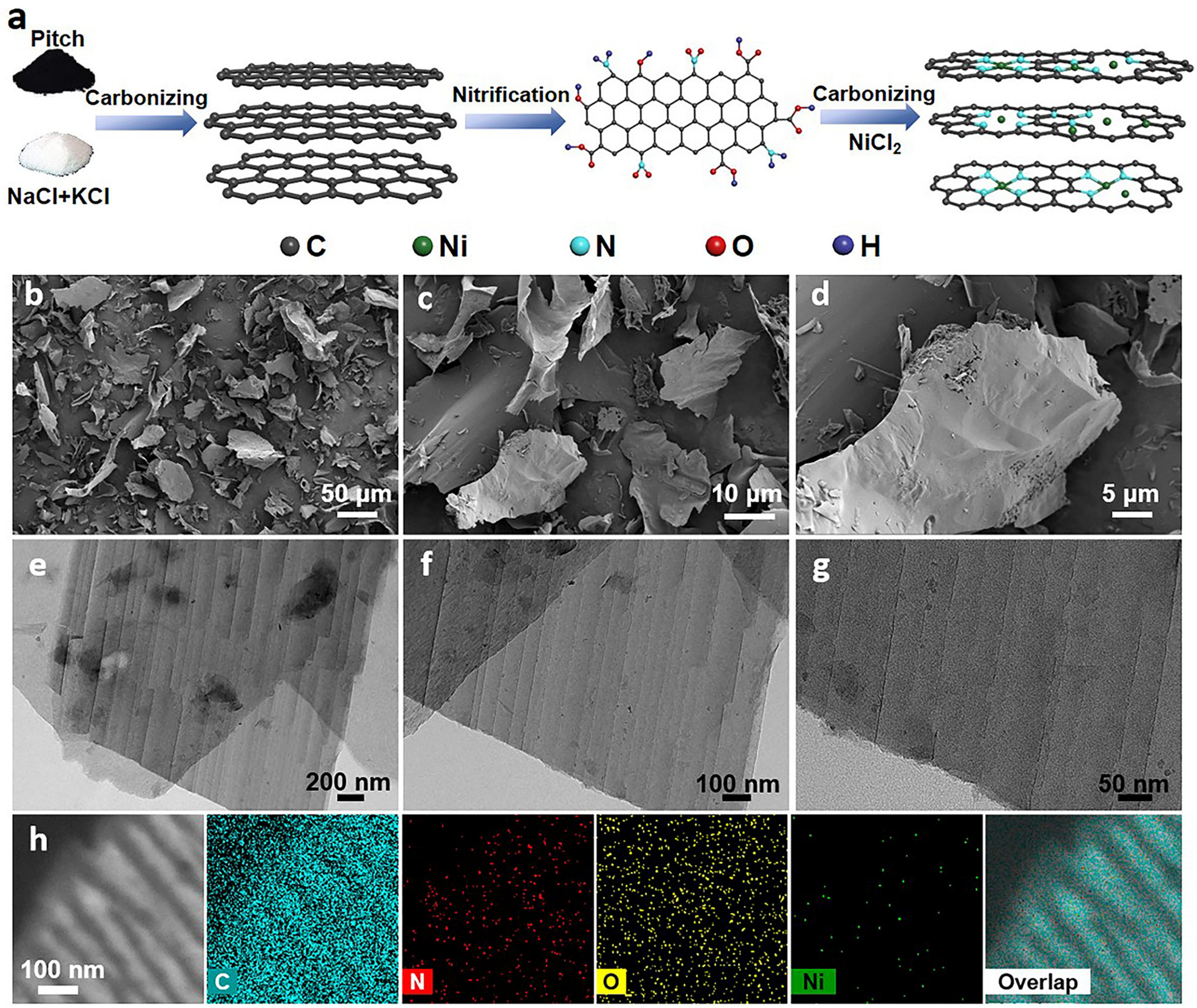

Fig. 1 (a) Schematic diagram of the synthetic procedure of the Ni/N–C catalysts. (b–d) SEM, (e–g) TEM and (h) EDS mapping images of Ni/N–C-900.

respectively. Obviously, the contents of both pyridinic-N and pyrrolic-N in the samples decrease by increasing the carbonization temperature. In contrast, the relative contents of graphitic-N in Ni/N–C-700, 800, 900 and 1000 are 21.2, 22.3, 24.2 and 31.7%, respectively. The possible reason is that the graphitic-N is more stable and is lost at a lower rate with the increasing temperature than the unstable pyridinic and pyrrolic-N. It is noteworthy that the relative content of Ni–N$_x$ reaches its maximum at 900 °C (30.6%), while higher carbonization temperature will reduce the number of Ni–N$_x$ species (1000 °C, 25.1%). All these results show that 900 °C is an optimum temperature for the formation of Ni–N$_x$ species (1.18 at%) and the maintenance of a high total nitrogen content (3.85 at%), which are beneficial for improving the catalytic performance. Thus, the number of Ni–N$_x$ active sites can be modulated by changing the carbonization temperature, thus further adjusting the H$_2$/CO ratios.[35,36] Although the main active sites in Ni/N–C catalysts are Ni–N$_x$ coordinated structures, graphitic-N, pyridinic-N and pyrrolic-N also play important roles in the CO$_2$RR, in which pyridinic-N is a dominant factor. Therefore, the Ni–N$_x$ active sites and N species have synergistic effects on the CO$_2$RR activity in the Ni/N–C electrocatalysts.[37,38]

The high-resolution spectra of Ni 2p are displayed in Fig. 2d, where the Ni 2p$_{3/2}$ peak at 855.5 eV is between those of Ni^0 (852.5–853.0 eV) and Ni^{2+} (856 eV),[39–41] revealing that the Ni species are in an unsaturated chemical state and the potential presence of coordinated Ni–N sites in the catalysts. In addition, the Ni contents were also detected by inductively coupled plasma-optical emission spectroscopy (ICP-OES), where the Ni/N–C-900 catalyst (0.00936 wt%) possesses higher Ni content than those of Ni/N–C-700 (0.00230 wt%), Ni/N–C-800 (0.00283 wt%) and Ni/N–C-1000 (0.00381 wt%) (Table S2†), which agrees well with the XPS results. The high-resolution N 1s and Ni 2p spectra of N–C and Ni–C samples are shown in Fig. S6,† demonstrating the absence of Ni–N$_x$ active sites. The trace amount of N species (0.00188 wt%) in

This journal is © the Partner Organisations 2023

Published on 10 March 2023. Downloaded on 7/15/2025 3:38:55 AM.

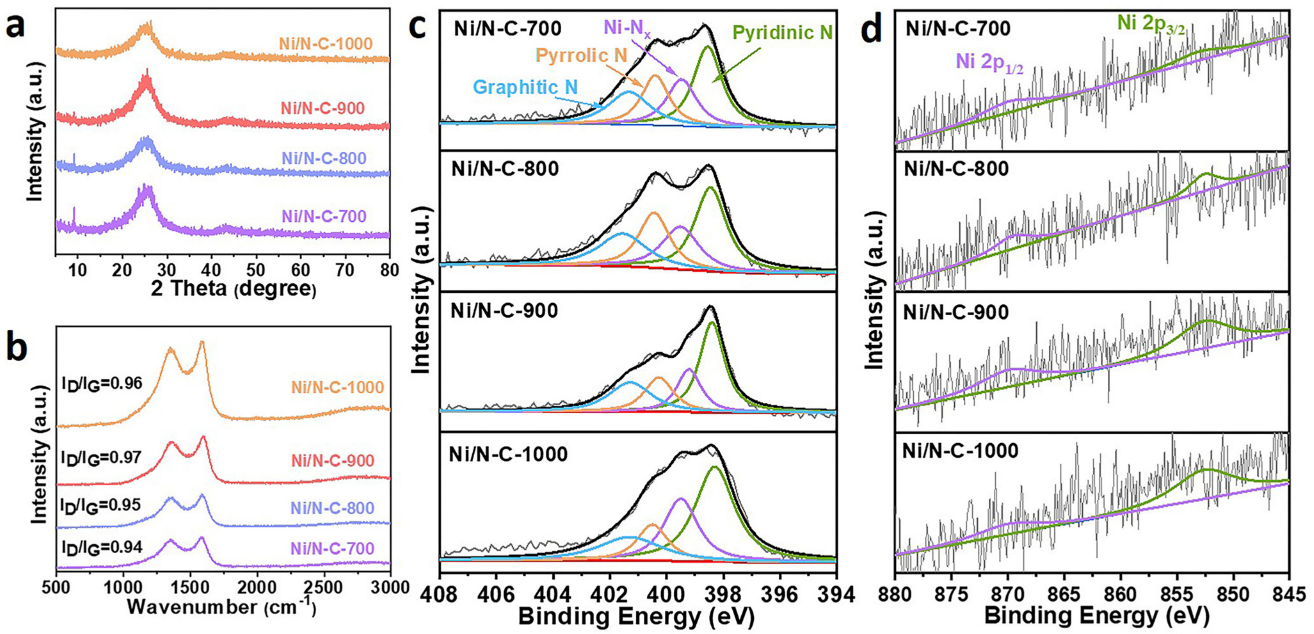

Fig. 2 (a) XRD patterns and (b) Raman spectra of various Ni/N–C catalysts. High-resolution XPS spectra of (c) N 1s and (d) Ni 2p in Ni/N–C-700, 800, 900 and 1000.

the Ni–C sample comes from coal tar pitch, which is insufficient to form Ni–N_x active sites with Ni sources.

The electrochemical activities of various electrocatalysts were investigated in an H-type cell. As revealed by linear sweep voltammetry (LSV) curves in Fig. 3a, the current densities of various catalysts under a CO_2 atmosphere are significantly higher than those of catalysts under an Ar atmosphere, proving their preference towards the CO_2RR. Compared with N–C (1.25 mA cm^{-2}) and Ni–C (1.47 mA cm^{-2}), Ni/N–C-900 exhibits higher current density (8.37 mA cm^{-2}) (Fig. S7a†), demonstrating that the ultrathin carbon nanosheets can promote the performance of the CO_2RR.[42] To determine the composition of the resulting syngas, the H_2/CO ratios of various samples are calculated at different potentials (Fig. 3b). Obviously, the controllable ratios of H_2/CO vary from 1/2 to 2/1, providing an opportunity for tunable syngas production. Notably, most of the H_2/CO ratios of each sample at different potentials are distributed in the optimal region (0.5–2), and the syngas contents in this interval are the key feedstocks for preparing multiple chemical products.[24,43–47] The H_2/CO ratios of N–C and Ni–C (Fig. S7b†) show that most of the ratios deviated from the optimal syngas region, further demonstrating that the presence of Ni–N_x active sites can improve the selectivity for CO and thereby modulate the H_2/CO ratios.

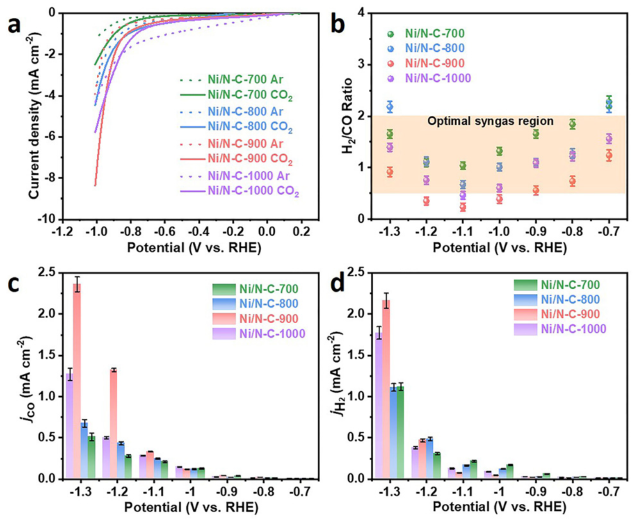

Fig. 3 (a) Linear sweep voltammetric (LSV) curves of various samples in CO_2 and Ar-saturated 0.1 M $KHCO_3$ solution. (b) Dependence of the H_2/CO ratio on the applied potentials of Ni/N–C-700, 800, 900 and 1000. Partial current densities of CO (c) and H_2 (d).

The CO partial current densities (j_{CO}) of various samples are 0.51 mA cm^{-2} (Ni/N–C-700), 0.68 mA cm^{-2} (Ni/N–C-800), 2.36 mA cm^{-2} (Ni/N–C-900), and 1.27 mA cm^{-2} (Ni/N–C-1000) (Fig. 3c). The j_{CO} of Ni/N–C catalysts is higher than that of N–C (0.24 mA cm^{-2}) and Ni–C (0.44 mA cm^{-2}) (Fig. S7†), suggesting that the Ni–N_x coordination structure plays a vital role in the CO_2RR. Meanwhile, the H_2 partial current densities (j_{H_2}) (Fig. 3d) and j_{CO} increase with the applied voltage; however, there are some differences in the magnitude of j_{H_2} and j_{CO} growth, indicating that the H_2/CO ratios of various Ni/N–C catalysts can also be modulated by changing the applied potential. The syngas production rate is also a key parameter for estimating the catalytic performance.

The production rates of CO and H_2 can vary with applied potentials (Fig. 4a and b). As predicted, the generation rates of CO and H_2 gradually increase in a wide potential window (−0.7 to −1.1 V *vs.* RHE). Ni/N–C-900 displays the maximum CO pro-

Published on 10 March 2023. Downloaded on 7/15/2025 3:38:55 AM.

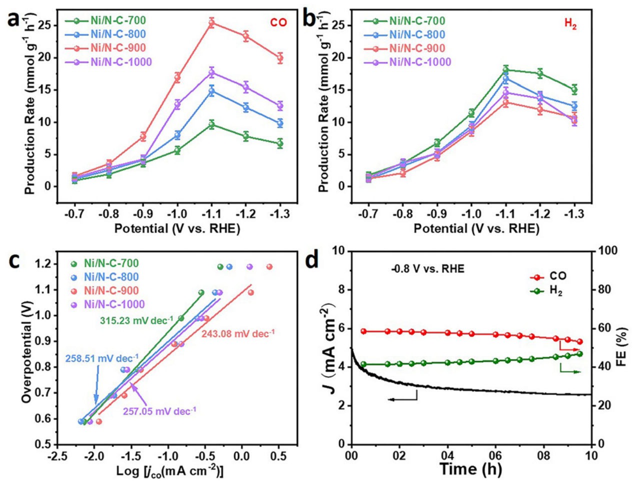

Fig. 4 (a) CO and (b) H_2 production rates of Ni/N–C catalysts at different applied potentials. (c) Tafel plots based on j_{CO} of the Ni/N–C catalysts in CO_2-saturated 0.1 M $KHCO_3$ solution. (d) Long-term stability test of Ni/N–C-900 at −0.8 V *vs.* RHE for 10 h.

duction rate (19.96 mmol g^{-1} h^{-1}) compared with those of Ni/N–C-700 (6.68 mmol g^{-1} h^{-1}), Ni/N–C-800 (9.83 mmol g^{-1} h^{-1}) and Ni/N–C-1000 (12.55 mmol g^{-1} h^{-1}), demonstrating that the production rates of CO are consistent with the number of Ni–N_x active sites. From 700 to 900 °C, the number of Ni–N_x active sites in the catalysts gradually increases, the reactions are mainly based on the CO_2RR, and the HER is inhibited, resulting in a gradual decrease of production rates for H_2. As the temperature continued to rise to 1000 °C, the decrease in the number of Ni–N_x active sites caused a gradually enhanced HER. To further reveal the reaction kinetics of the catalysts, the Tafel slopes for CO production over Ni/N–C catalysts are presented in Fig. 4c. The Tafel slope of Ni/N–C-900 is 243.08 mV dec^{-1}, which is lower than those of Ni/N–C-700 (315.23 mV dec^{-1}), Ni/N–C-800 (258.51 mV dec^{-1}) and Ni/N-C-1000 (257.05 mV dec^{-1}), implying that the increased number of Ni–N_x active sites accelerates the reaction kinetics.[48] Meanwhile, the Tafel slopes of Ni/N–C catalysts are significantly lower than those of N–C (322.85 mV dec^{-1}) and Ni–C (319.59 mV dec^{-1}) (Fig. S8†), further proving that the Ni–N_x active sites can accelerate the reaction kinetics of Ni/N–C catalysts in the CO_2RR.[49,50]

In addition, Fig. S9 and S10† show the electrochemically active surface areas (ECSAs) and the double-layer capacitances (C_{dl}) of all samples. The C_{dl} of Ni/N–C-900 (1.08 mF cm^{-2}) is obviously larger than the C_{dl} of Ni/N–C-700 (0.613 mF cm^{-2}), Ni/N–C-800 (0.842 mF cm^{-2}), Ni/N–C-1000 (0.863 mF cm^{-2}), N–C (0.365 mF cm^{-2}) and Ni–C (0.426 mF cm^{-2}). The results show that the ESCA of Ni/N–C-900 is the largest among the above samples, which is conducive to increasing the contact area between active sites and CO_2. The j_{CO} of different catalysts is normalized to the ECSA to fairly compare the catalytic activity of Ni/N–C-900 with other samples. As shown in Fig. S11,† Ni/N–C-900 displays a significantly larger ESCA-normalized CO current density than the N–C and Ni–C samples. Thus, the higher intrinsic activity of Ni/N–C-900 is attributed to its unique Ni–N_x sites. An isotope tracer measurement for the electroreduction of $^{13}CO_2$ was carried out to trace the origin of the products, where $^{12}CO_2$ was used as a reference. As shown in Fig. S12,† the dominant peak of ^{13}CO ($m/z = 29$) was observed at m/z = 29, which was assigned to ^{13}CO produced during the MS measurement. The results verify that CO detected upon the Ni/N–C materials comes from the electroreduction of the CO_2 source instead of any organic impurities from the catalyst. Furthermore, Ni/N–C-900 exhibits significant electrochemical stability in a long-term electrolysis test. When the reaction continues for 10 h at −0.8 V *vs.* RHE, the H_2/CO ratio remains basically stable and the current density decreases only slightly at the beginning (Fig. 4d). At the beginning of the reaction, sufficient CO_2 is adsorbed on the electrode and a large amount of CO_2 is consumed instantaneously after applying the potential. However, as the reaction proceeds, the insufficient supply of CO_2 leads to a decrease in the current density. To verify the reason for the decrease of FE_{co} after 10 h of electrolysis, we investigated the chemical states of N species. The relative contents of various N dopants show no obvious differences compared with the fresh Ni/N–C-900 sample. However, the atomic concentration of total N decreases from 3.85 to 3.02 at% (Fig. S13†), which may be the cause of deactivation.

In order to highlight the advantages of the stable and controlled syngas production within a wide potential window over the Ni–N co-doped ultrathin carbon nanosheet electrodes, a comparison between H_2/CO ratios in this work and those in recent representative literature reports is presented in Fig. 5.

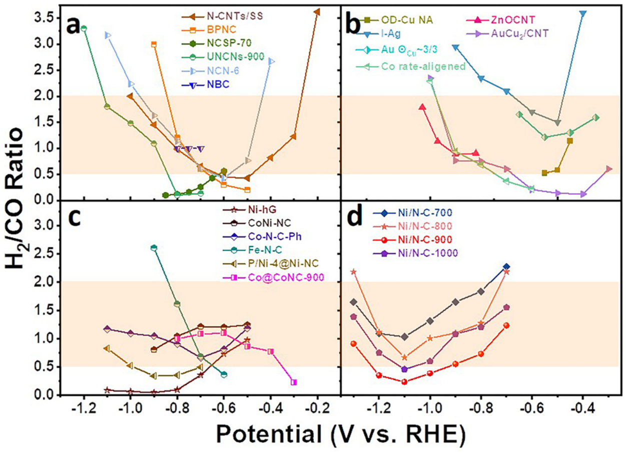

Fig. 5 Recently reported H_2/CO ratios of various catalysts used for syngas production at different applied potentials. (a) Heteroatom-doped carbon catalysts (N-CNTs,[42] BPNC,[14] NCSP-70,[51] UNCNs-900,[52] NCN-6,[53] and NBC[54]), (b) metal catalysts (OD-Cu NA,[55] ZnOCNT,[56] I-Ag,[57] $AuCu_2$/CNT,[58]Au Θ_{Cu} ~ 3/3,[59] and Co rate-aligened[60]), (c) M–N–C single-atom catalysts (Ni-hG,[23] CoNi-NC,[24] Co–N–C–Ph,[61] Fe–N–C,[33] P/Ni-4@Ni-NC,[62] and Co@CoNC-900 [63]) and (d) Ni–N co-doped ultrathin carbon nanosheet electrodes. The shaded regions are the areas with the optimal syngas ratios.

Published on 10 March 2023. Downloaded on 7/15/2025 3:38:55 AM.

The H_2/CO ratios over heteroatom-doped carbon catalysts and metal catalysts could be regulated in the range of 0–3.5, but it is far from the optimal range. Meanwhile, the weak intrinsic activity of heteroatom-doped carbon and the scarcity or cost disadvantages of metal catalysts still limit their large-scale application. Compared with the M–N–C catalysts in the literature, our Ni/N–C catalysts showed obvious advantages in the regulatory range, that is, it covered all the optimal syngas regions. Furthermore, the ratio of syngas on our catalysts can be controlled simultaneously by adjusting the active site content and applied potential. The unique and convenient regulation strategy of this work enables the H_2/CO ratio to be adjusted between 1/2 and 2/1 within a wide voltage window, highlighting excellent intrinsic activity and economy.

Conclusions

In summary, this work presented Ni–N co-doped carbon nanosheets as promising catalysts for the electrochemical conversion of CO_2 to tunable syngas. The number of Ni–N active sites in the catalysts is varied by adjusting the carbonization temperature of the synthesis process, enabling the effective regulation of H_2/CO ratios to the optimal range (1/2–2/1) over a wide potential window (from −0.7 to −1.3 V *vs.* RHE). The scheme of modulating the H_2/CO ratios by changing the number of $Ni–N_x$ active sites shows great potential and may provide a valuable reference for future syngas production.

Author contributions

Kaining Gan: investigation, methodology, data curation, writing – original draft, review and editing. Hongqiang Li: supervision, conceptualization, methodology, writing – review and editing, and funding acquisition. Ran Li: investigation and validation. Jiabao Niu: investigation and methodology. Jun He: validation. Dedong Jia: review and editing, and funding acquisition. Xiaojun He: supervision and funding acquisition.

Conflicts of interest

There are no conflicts of interest to declare.

Acknowledgements

This work was partly supported by the National Natural Science Foundation of China [no. 22108003, 52072002, 51872005, 52002194], the Natural Science Foundation of Anhui Provincial Education Department [no. KJ2020A0254], the Research Fund for Young Teachers of Anhui University of Technology [no. QZ202007], and the Wanjiang Scholar Program. The authors would also like to acknowledge the financial support from the Anhui International Research Center of Energy Materials Green Manufacturing and Biotechnology.

References

1 J. M. Spurgeon and B. Kumar, A comparative technoeconomic analysis of pathways for commercial electrochemical CO_2 reduction to liquid products, *Energy Environ. Sci.*, 2018, **11**, 1536–1551.
2 J. Hao, Z. Zhuang, J. Hao, K. Cao, Y. Hu, W. Wu, S. Lu, C. Wang, N. Zhang, D. Wang, M. Du and H. Zhu, Strain Relaxation in Metal Alloy Catalysts Steers the Product Selectivity of Electrocatalytic CO_2 Reduction, *ACS Nano*, 2022, **16**, 3251–3263.
3 F. Naseem, P. Lu, J. Zeng, Z. Lu, Y. H. Ng, H. Zhao, Y. Du and Z. Yin, Solid Nanoporosity Governs Catalytic CO_2 and N_2 Reduction, *ACS Nano*, 2020, **14**, 7734–7759.
4 Z. Yin, J. Yu, Z. Xie, S.-W. Yu, L. Zhang, T. Akauola, J. G. Chen, W. Huang, L. Qi and S. Zhang, Hybrid Catalyst Coupling Single-Atom Ni and Nanoscale Cu for Efficient CO_2 Electroreduction to Ethylene, *J. Am. Chem. Soc.*, 2022, **144**, 20931–20938.
5 H. Li, R. Li, J. Niu, K. Gan and X. He, Defect chemistry of electrocatalysts for CO_2 reduction, *Front. Chem.*, 2022, **10**, 1067327.
6 H. Li, N. Xiao, M. Hao, X. Song, Y. Wang, Y. Ji, C. Liu, C. Li, Z. Guo, F. Zhang and J. Qiu, Efficient CO_2 electroreduction over pyridinic-N active sites highly exposed on wrinkled porous carbon nanosheets, *Chem. Eng. J.*, 2018, **351**, 613–621.
7 H. Li, X. He, T. Wu, B. Jin, L. Yang and J. Qiu, Synthesis, modification strategies and applications of coal-based carbon materials, *Fuel Process. Technol.*, 2022, **230**, 107203.
8 Y. Jiang, R. Long and Y. Xiong, Regulating C–C coupling in thermocatalytic and electrocatalytic COx conversion based on surface science, *Chem. Sci.*, 2019, **10**, 7310–7326.
9 Y. Liu, D. Tian, A. N. Biswas, Z. Xie, S. Hwang, J. H. Lee, H. Meng and J. G. Chen, Transition Metal Nitrides as Promising Catalyst Supports for Tuning CO/H_2 Syngas Production from Electrochemical CO_2 Reduction, *Angew. Chem., Int. Ed.*, 2020, **59**, 11345–11348.
10 Y. E. Kim, B. Kim, W. Lee, Y. N. Ko, M. H. Youn, S. K. Jeong, K. T. Park and J. Oh, Highly tunable syngas production by electrocatalytic reduction of CO_2 using Ag/TiO_2 catalysts, *Chem. Eng. J.*, 2021, **413**, 127448.
11 H. He, D. Xia, X. Yu, J. Wu, Y. Wang, L. Wang, L. Wu, J. Huang, N. Zhao, L. Deng and Y.-N. Liu, Pd-SnO_2 interface enables synthesis of syngas with controllable H_2/CO ratios by electrocatalytic reduction of CO_2, *Appl. Catal. B-Environ.*, 2022, **312**, 121392.
12 J. Y. Maeng, J. H. Yang, H. J. Jang, M. H. Joo, Y. J. Kim, C. K. Rhee and Y. Sohn, Electrocatalytic syngas and photocatalytic long-chain hydrocarbon productions by CO_2 reduction over ZnO and Zn-based electrodes, *Appl. Surf. Sci.*, 2023, **609**, 155349.
13 P. Chen, Y. Jiao, Y.-H. Zhu, S.-M. Chen, L. Song, M. Jaroniec, Y. Zheng and S.-Z. Qiao, Syngas production from electrocatalytic CO_2 reduction with high energetic

Published on 10 March 2023. Downloaded on 7/15/2025 3:38:55 AM.

efficiency and current density, *J. Mater. Chem. A*, 2019, **7**, 7675–7682.

14 J. Han, X. Deng, K. Chen, S. Imhanria, Y. Sun and W. Wang, Electrochemical conversion of CO_2 into tunable syngas on a B, P, N tri-doped carbon, *Renewable Energy*, 2021, **177**, 636–642.

15 H. Li, N. Xiao, Y. Wang, C. Li, X. Ye, Z. Guo, X. Pan, C. Liu, J. Bai, J. Xiao, X. Zhang, S. Zhao and J. Qiu, Nitrogen-doped tubular carbon foam electrodes for efficient electroreduction of CO_2 to syngas with potential-independent CO/H_2 ratios, *J. Mater. Chem. A*, 2019, **7**, 18852–18860.

16 T. Wang, Q. Zhao, Y. Fu, C. Lei, B. Yang, Z. Li, L. Lei, G. Wu and Y. Hou, Carbon-Rich Nonprecious Metal Single Atom Electrocatalysts for CO_2 Reduction and Hydrogen Evolution, *Small Methods*, 2019, **3**, 1900210.

17 F. Pan, W. Deng, C. Justiniano and Y. Li, Identification of champion transition metals centers in metal and nitrogen-codoped carbon catalysts for CO_2 reduction, *Appl. Catal. B-Environ.*, 2018, **226**, 463–472.

18 A. S. Varela, W. Ju and P. Strasser, Molecular Nitrogen–Carbon Catalysts, Solid Metal Organic Framework Catalysts, and Solid Metal/Nitrogen-Doped Carbon (MNC) Catalysts for the Electrochemical CO_2 Reduction, *Adv. Energy Mater.*, 2018, **8**, 1703614.

19 H. Tao, C. Choi, L.-X. Ding, Z. Jiang, Z. Han, M. Jia, Q. Fan, Y. Gao, H. Wang, A. W. Robertson, S. Hong, Y. Jung, S. Liu and Z. Sun, Nitrogen Fixation by Ru Single-Atom Electrocatalytic Reduction, *Chem*, 2019, **5**, 204–214.

20 J. Zhao, Y. Zhang, X. Kang and Y. Li, The preparation of NiO/Ni–N/C nanocomposites and its electrocatalytic performance for methanol oxidation reaction, *New J. Chem.*, 2020, **44**, 14970–14978.

21 W. Bi, X. Li, R. You, M. Chen, R. Yuan, W. Huang, X. Wu, W. Chu, C. Wu and Y. Xie, Surface Immobilization of Transition Metal Ions on Nitrogen-Doped Graphene Realizing High-Efficient and Selective CO_2 Reduction, *Adv. Mater.*, 2018, **30**, 1706617.

22 W.-j. Wang, C. Cao, K. Wang and T. Zhou, Boosting CO_2 electroreduction to CO with abundant nickel single atom active sites, *Inorg. Chem. Front.*, 2021, **8**, 2542–2548.

23 J. Leverett, R. Daiyan, L. Gong, K. Iputera, Z. Tong, J. Qu, Z. Ma, Q. Zhang, S. Cheong, J. Cairney, R.-S. Liu, X. Lu, Z. Xia, L. Dai and R. Amal, Designing Undercoordinated $Ni–N_x$ and $Fe–N_x$ on Holey Graphene for Electrochemical CO_2 Conversion to Syngas, *ACS Nano*, 2021, **15**, 12006–12018.

24 Q. He, D. Liu, J. H. Lee, Y. Liu, Z. Xie, S. Hwang, S. Kattel, L. Song and J. G. Chen, Electrochemical Conversion of CO_2 to Syngas with Controllable CO/H_2 Ratios over Co and Ni Single-Atom Catalysts, *Angew. Chem., Int. Ed.*, 2020, **59**, 3033–3037.

25 C. Lu, J. Yang, S. Wei, S. Bi, Y. Xia, M. Chen, Y. Hou, M. Qiu, C. Yuan, Y. Su, F. Zhang, H. Liang and X. Zhuang, Atomic Ni Anchored Covalent Triazine Framework as High Efficient Electrocatalyst for Carbon Dioxide Conversion, *Adv. Funct. Mater.*, 2019, **29**, 1806884.

26 Q. Wu, J. Gao, J. Feng, Q. Liu, Y. Zhou, S. Zhang, M. Nie, Y. Liu, J. Zhao, F. Liu, J. Zhong and Z. Kang, A CO_2 adsorption dominated carbon defect-based electrocatalyst for efficient carbon dioxide reduction, *J. Mater. Chem. A*, 2020, **8**, 1205–1211.

27 C. Yan, H. Li, Y. Ye, H. Wu, F. Cai, R. Si, J. Xiao, S. Miao, S. Xie, F. Yang, Y. Li, G. Wang and X. Bao, Coordinatively unsaturated nickel–nitrogen sites towards selective and high-rate CO_2 electroreduction, *Energy Environ. Sci.*, 2018, **11**, 1204–1210.

28 C.-Z. Yuan, L.-Y. Zhan, S.-J. Liu, F. Chen, H. Lin, X.-L. Wu and J. Chen, Semi-sacrificial template synthesis of single-atom Ni sites supported on hollow carbon nanospheres for efficient and stable electrochemical CO_2 reduction, *Inorg. Chem. Front.*, 2020, **7**, 1719–1725.

29 S. Li, X. Lu, S. Zhao, M. Ceccato, X.-M. Hu, A. Roldan, M. Liu and K. Daasbjerg, p-Block Indium Single-Atom Catalyst with Low-Coordinated In–N Motif for Enhanced Electrochemical CO_2 Reduction, *ACS Catal.*, 2022, **12**, 7386–7395.

30 Y. Gang, F. Pan, Y. Fei, Z. Du, Y. H. Hu and Y. Li, Highly Efficient Nickel, Iron, and Nitrogen Codoped Carbon Catalysts Derived from Industrial Waste Petroleum Coke for Electrochemical CO_2 Reduction, *ACS Sustainable Chem. Eng.*, 2020, **8**, 8840–8847.

31 N. Zhang, T. Zhou, M. Chen, H. Feng, R. Yuan, C. a. Zhong, W. Yan, Y. Tian, X. Wu, W. Chu, C. Wu and Y. Xie, High-purity pyrrole-type FeN_4 sites as a superior oxygen reduction electrocatalyst, *Energy Environ. Sci.*, 2020, **13**, 111–118.

32 E. Lepre, J. Heske, M. Nowakowski, E. Scoppola, I. Zizak, T. Heil, T. D. Kühne, M. Antonietti, N. López-Salas and J. Albero, Ni-based electrocatalysts for unconventional CO_2 reduction reaction to formic acid, *Nano Energy*, 2022, **97**, 107191.

33 J. Zhao, J. Deng, J. Han, S. Imhanria, K. Chen and W. Wang, Effective tunable syngas generation via CO_2 reduction reaction by non-precious Fe-N-C electrocatalyst, *Chem. Eng. J.*, 2020, **389**, 124323.

34 F. Chang, Y. Ma, P. Su and J. Liu, Synthesis of a graphitized hierarchical porous carbon material supported with a transition metal for electrochemical conversion, *Inorg. Chem. Front.*, 2022, **9**, 1794–1801.

35 Q. Lai, L. Zheng, Y. Liang, J. He, J. Zhao and J. Chen, Metal–Organic-Framework-Derived Fe-N/C Electrocatalyst with Five-Coordinated $Fe-N_x$ Sites for Advanced Oxygen Reduction in Acid Media, *ACS Catal.*, 2017, **7**, 1655–1663.

36 Z. Ma, X. Zhang, D. Wu, X. Han, L. Zhang, H. Wang, F. Xu, Z. Gao and K. Jiang, Ni and nitrogen-codoped ultrathin carbon nanosheets with strong bonding sites for efficient CO_2 electrochemical reduction, *J. Colloid Interface Sci.*, 2020, **570**, 31–40.

37 M. Jia, C. Choi, T.-S. Wu, C. Ma, P. Kang, H. Tao, Q. Fan, S. Hong, S. Liu, Y.-L. Soo, Y. Jung, J. Qiu and Z. Sun, Carbon-supported Ni nanoparticles for efficient CO_2 electroreduction, *Chem. Sci.*, 2018, **9**, 8775–8780.

This journal is © the Partner Organisations 2023

Published on 10 March 2023. Downloaded on 7/15/2025 3:38:55 AM.

38 X. Tan, C. Yu, S. Cui, L. Ni, W. Guo, Z. Wang, J. Chang, Y. Ren, J. Yu, H. Huang and J. Qiu, Activity descriptor of Ni, N-Codoped carbon electrocatalyst in CO_2 electroreduction reaction, *Chem. Eng. J.*, 2022, **433**, 131965.

39 F. Pan, B. Li, E. Sarnello, Y. Fei, X. Feng, Y. Gang, X. Xiang, L. Fang, T. Li, Y. H. Hu, G. Wang and Y. Li, Pore-Edge Tailoring of Single-Atom Iron–Nitrogen Sites on Graphene for Enhanced CO_2 Reduction, *ACS Catal.*, 2020, **10**, 10803–10811.

40 Y.-N. Gong, L. Jiao, Y. Qian, C.-Y. Pan, L. Zheng, X. Cai, B. Liu, S.-H. Yu and H.-L. Jiang, Regulating the Coordination Environment of MOF-Templated Single-Atom Nickel Electrocatalysts for Boosting CO_2 Reduction, *Angew. Chem., Int. Ed.*, 2020, **59**, 2705–2709.

41 H. Cheng, X. Wu, X. Li, Y. Zhang, M. Feng, Z. Fan and G. He, Zeolitic imidazole framework-derived FeN_5-doped carbon as superior CO_2 electrocatalysts, *J. Catal.*, 2021, **395**, 63–69.

42 K.-H. Liu, H.-X. Zhong, X.-Y. Yang, D. Bao, F.-L. Meng, J.-M. Yan and X.-B. Zhang, Composition-tunable synthesis of "clean" syngas via a one-step synthesis of metal-free pyridinic-N-enriched self-supported CNTs: the synergy of electrocatalyst pyrolysis temperature and potential, *Green Chem.*, 2017, **19**, 4284–4288.

43 A. Kamiyama, K. Kubota, T. Nakano, S. Fujimura, S. Shiraishi, H. Tsukada and S. Komaba, High-Capacity Hard Carbon Synthesized from Macroporous Phenolic Resin for Sodium-Ion and Potassium-Ion Battery, *ACS Appl. Energy Mater.*, 2020, **3**, 135–140.

44 L. Xiong, X. Zhang, L. Chen, Z. Deng, S. Han, Y. Chen, J. Zhong, H. Sun, Y. Lian, B. Yang, X. Yuan, H. Yu, Y. Liu, X. Yang, J. Guo, M. H. Rümmeli, Y. Jiao and Y. Peng, Geometric Modulation of Local CO Flux in Ag@Cu_2O Nanoreactors for Steering the CO_2RR Pathway toward High-Efficacy Methane Production, *Adv. Mater.*, 2021, **33**, 2101741.

45 B. Ren, Z. Zhang, G. Wen, X. Zhang, M. Xu, Y. Weng, Y. Nie, H. Dou, Y. Jiang, Y.-P. Deng, G. Sun, D. Luo, L. Shui, X. Wang, M. Feng, A. Yu and Z. Chen, Dual-Scale Integration Design of Sn–ZnO Catalyst toward Efficient and Stable CO_2 Electroreduction, *Adv. Mater.*, 2022, **34**, 2204637.

46 J. Zhu, M. Xiao, D. Ren, R. Gao, X. Liu, Z. Zhang, D. Luo, W. Xing, D. Su, A. Yu and Z. Chen, Quasi-Covalently Coupled Ni–Cu Atomic Pair for Synergistic Electroreduction of CO_2, *J. Am. Chem. Soc.*, 2022, **144**, 9661–9671.

47 W. Yang, J.-H. Zhang, R. Si, L.-M. Cao, D.-C. Zhong and T.-B. Lu, Efficient and steady production of 1 : 2 syngas (CO/H_2) by simultaneous electrochemical reduction of CO_2 and H_2O, *Inorg. Chem. Front.*, 2021, **8**, 1695–1701.

48 H. Li, K. Gan, R. Li, H. Huang, J. Niu, Z. Chen, J. Zhou, Y. Yu, J. Qiu and X. He, Highly Dispersed NiO Clusters Induced Electron Delocalization of Ni-N-C Catalysts for Enhanced CO_2 Electroreduction, *Adv. Funct. Mater.*, 2023, **33**, 2208622.

49 P. Ding, H. Zhao, T. Li, Y. Luo, G. Fan, G. Chen, S. Gao, X. Shi, S. Lu and X. Sun, Metal-based electrocatalytic conversion of CO_2 to formic acid/formate, *J. Mater. Chem. A*, 2020, **8**, 21947–21960.

50 X. Zhong, S. Liang, T. Yang, G. Zeng, Z. Zhong, H. Deng, L. Zhang and X. Sun, Sn Dopants with Synergistic Oxygen Vacancies Boost CO_2 Electroreduction on CuO Nanosheets to CO at Low Overpotential, *ACS Nano*, 2022, **16**, 19210–19219.

51 Y. Shang, Y. Ding, P. Zhang, M. Wang, Y. Jia, Y. Xu, Y. Li, K. Fan and L. Sun, Pyrrolic N or pyridinic N: The active center of N-doped carbon for CO_2 reduction, *Chin. J. Catal.*, 2022, **43**, 2405–2413.

52 B. Wei, J. Hao, B. Ge, W. Luo, Y. Chen, Y. Xiong, L. Li and W. Shi, Highly efficient electrochemical carbon dioxide reduction to syngas with tunable ratios over pyridinic-nitrogen rich ultrathin carbon nanosheets, *J. Colloid Interface Sci.*, 2022, **608**, 2650–2659.

53 J. Gui, K. Zhang, X. Zhan, Y. Yu, T. Huang, Y. Li, J. Xue, X. Jin, S. Gao and Y. Xie, Nitrogen-doped porous carbon nanosheets as a robust catalyst for tunable CO_2 electroreduction to syngas, *Sustain. Energy Fuels*, 2022, **6**, 1512–1518.

54 X. Ma, L. Shi, L. Zhang, C. Hu and D. Liu, Tuning B–N pairs in porous carbon nanorods for electrochemical conversion of CO_2 to syngas with controllable CO/H_2 ratios, *Sustain. Energy Fuels*, 2023, **7**, 661–670.

55 Y. Wang, C. Niu, Y. Zhu, D. He and W. Huang, Tunable Syngas Formation from Electrochemical CO_2 Reduction on Copper Nanowire Arrays, *ACS Appl. Energy Mater.*, 2020, **3**, 9841–9847.

56 I. Hjorth, Y. Wang, Y. Li, M. E. M. Buan, M. Nord, M. Rønning, J. Yang and D. Chen, Electrochemical syngas production from CO_2 and water with CNT supported ZnO catalysts, *Catal. Today*, 2021, **364**, 172–181.

57 H. Li, J. Gao, J. Shan, Q. Du, Y. Zhang, X. Guo, M. Xie, S. Wu and Z. Wang, Effect of halogen-modification on Ag catalyst for CO_2 electrochemical reduction to syngas from NH_4HCO_3 electrolyte, *J. Environ. Chem. Eng.*, 2021, **9**, 106415.

58 H. Chen, Z. Li, Z. Zhang, K. Jie, J. Li, H. Li, S. Mao, D. Wang, X. Lu and J. Fu, Synthesis of Composition-Tunable Syngas from Efficiently Electrochemical Conversion of CO_2 over AuCu/CNT Bimetallic Catalyst, *Ind. Eng. Chem. Res.*, 2019, **58**, 15425–15431.

59 M. B. Ross, C. T. Dinh, Y. Li, D. Kim, P. De Luna, E. H. Sargent and P. Yang, Tunable Cu Enrichment Enables Designer Syngas Electrosynthesis from CO_2, *J. Am. Chem. Soc.*, 2017, **139**, 9359–9363.

60 M. B. Ross, Y. Li, P. De Luna, D. Kim, E. H. Sargent and P. Yang, Electrocatalytic Rate Alignment Enhances Syngas Generation, *Joule*, 2019, **3**, 257–264.

61 Z. Guo, Q. Zhang, F. Shen, H. Liu, H. Zhang, Z. Guo, B. Jin and R. Peng, Boosting electron transport over controllable N ligand doping for electrochemical conversion of CO_2 to syngas, *Electrochim. Acta*, 2021, **388**, 138647.

Published on 10 March 2023. Downloaded on 7/15/2025 3:38:55 AM.

62 C. Ye, X. Yu, W. Li, L. He, G. Hao and A. Lu, Engineering of Bifunctional Nickel Phosphide@Ni-N-C Catalysts for Selective Electroreduction of CO_2-H_2O to Syngas, *Acta Phys.-Chim. Sin.*, 2022, **38**, 2004054.

63 R. Daiyan, R. Chen, P. Kumar, N. M. Bedford, J. Qu, J. M. Cairney, X. Lu and R. Amal, Tunable Syngas Production through CO_2 Electroreduction on Cobalt–Carbon Composite Electrocatalyst, *ACS Appl. Mater. Interfaces*, 2020, **12**, 9307–9315.